IIETA International Information and Engineering Technology Association
Advancing the World of Information and Engineering

Mathematical Modelling of Engineering Problems
Vol. 9, No. 5, October, 2022, pp. 1161-1171
Journal homepage: http://iieta.org/journals/mmep

Capacitance Calculation Model in Corona Discharge Case

Asep Yoyo Wardaya[1*], Zaenul Muhlisin[1], Jatmiko Endro Suseno[1], Charis Munajib[1], Susilo Hadi[2], Heri Sugito[1], Jaka Windarta[3]

[1] Department of Physics, Faculty of Science and Mathematics, Diponegoro University, Semarang 50275, Indonesia
[2] M1 Physique, Facult é de Sciences, Université d'Aix-Marseille, Marseille 13331, France
[3] Department of Electrical Engineering, Faculty of Engineering, Diponegoro University, Semarang 50275, Indonesia

Corresponding Author Email: asepyoyowardayafisika@gmail.com

https://doi.org/10.18280/mmep.090501

Received: 17 August 2022
Accepted: 4 October 2022

Keywords:
corona discharge, (I-V) characteristics, CEM-P, shape sharpness factor, python GUI programming

ABSTRACT

The (*I-V*) characteristic pattern of the corona discharge case is very different from the pattern of ordinary electric circuits, so it is interesting to investigate. Several previous studies involved the concept of Maxwell's equations on several physical case models such as coaxial cylinder, electrohydrodynamic, and the electric wind. In this study, we use a capacitance calculation model for positive dc corona discharge in air, especially in calculating the (*I-V*) current-voltage characteristics of an electrode configuration model, often referred to as capacitively coupled plasma (CCP). The configuration model comprises active and passive electrodes, with the active electrode in the form of a pentagonal with the sharp end (in the middle) facing downwards in an upright position. The passive electrode under the active electrode has a large rectangular shape in a lying place. This configuration model is named The Chisel Eye and Midpoint-Plane (CEM-P). The analytical calculation of the (*I-V*) characteristics uses the geometric properties of the active electrode, which will produce a large corona current flow at the pointed electrode. These properties in analytical calculation manifest with the emergence of the corona flow multiplication factor at the sharp active electrode's integration boundary condition called the shape sharpness factor k. The Python GUI Programming simulation program makes graphic simulations, Standard Deviation (*SD*), t-tests, and calculating the factor *k* (fitting curve value) between numerical calculations and research data. The values of the *SD*, the t-tests, and the Percentage of tangent points meet the requirements for a high level of accuracy for the four CEM-P configuration models of the (*I-V*) characteristics simulation graph with the graph has a relatively large percentage of tangent points values (82.35% – 94.44%).

1. INTRODUCTION

The development of cold plasma technology had a positive impact on the industry, especially for use in electronic equipment with plasma temperatures that are not too high but produce a high enough technological leap through an equipment model called capacitively coupled plasma (CCP) [1]. Cold plasma is characterised by the temperature of the heavy species (particles and neutral ions) close to room temperature (25℃-100℃). This condition becomes important when irradiating materials sensitive to high temperatures [2], such as those used in CCP equipment or materials radiated by the CCP equipment.

The CCP model uses the concept of corona plasma discharge with an electrode configuration consisting of an active electrode in a vertical position and a passive electrode in a horizontal position (under the active electrode). The active electrode has a sharp-shaped surface towards the bottom. The passive electrode has a large surface to accommodate all the plasma flow from the active electrode. The CCP equipment is similar to the capacitance equipment with the position of the two electrodes perpendicular to each other [3]. If the CCP equipment connects to a dc voltage source, it can produce a corona plasma discharge under the appropriate voltage conditions.

The (*I-V*) current-voltage characteristic in the corona plasma discharge is an exciting research topic. This topic involves a variety of physical properties that cause Townsend's low current to appear, followed by a reasonably high current increase in corona discharge and arc discharge events [4]. Various studies explain the characteristic current-voltage phenomenon in the corona discharge, including the coaxial cylinders model [5, 6], the electro-hydrodynamics model [7], and the Electric Wind model [8]. Similarly, the application of CCP equipment has helped the development of research in other fields or used for industries such as ultra-large-scale integrated circuit (ULSI) fabrication [9], surface modification of polymeric materials [10], Large-area coating [11], lens-shaped electrodes [12], AC dielectric barrier discharges [13], etc.

In 2020, Wardaya et al. [14] make another form of the (I-V) characteristic related to the geometric function of the CCP electrode model. The geometric part has also been discussed [8] to compare the corona current function and the voltage's square function. In the research [14, 15], the geometric part comes from the modified capacitance function by adding a multiplier factor *k* to the sharp surface of the active electrode. The value of factor *k* came from the suitability factor between

the analytical formulation and the experimental results (curve fitting value). The factor k is the shape sharpness factor, which came from calculating the capacitance through the insertion of the integration limit on the part of the active electrode with a sharp surface. The ideal value of k will be higher if the shape of the active electrode is more tapered. The presence of the factor k came from the research results from Dobranszky et al. [16], who proved that the pointed tip of the active electrode (with a variety of sharpness angles and different materials) would look the plasma discharge brighter and more significant.

This research discusses the calculation of the (*I-V*) characteristic of positive dc corona discharge in the air (the CCP model) using The Chisel Eye and Midpoint-Plane (CEM-P) electrodes configuration models. Zheng et al. [6], Guan et al. [7], Robinson [8] uses the electric field concept from Maxwell's equation applied to the coaxial cylinder model, the continuity equation of electrohydrodynamic, and the electric wind, respectively. This study does not use a physical approach from Maxwell's equations but a geometric approach from the active electrode tip of the capacitor, which gives rise to the shape sharpness factor of k [14, 15]. Wardaya et al. [14] used an active electrode tip approach in the form of a sharp line, Wardaya et al. [15] using a sharp semicircular active electrode shape with pointed left and right sides. This study uses the tip of the active electrode as a sharp and pointed triangle. The pointed angle at the tip of the active electrode is $\phi=2\theta$. This study uses variations in the angle θ not found [14, 15] and variations in the distance between the two electrodes. This study is significant. We will be able to calculate the variation of electric current and plasma discharge required from the electrode model (*CCP* equipment) only by using the given voltage variation and variations in the length and angle of sharpness of the active electrode at a specific value of k. This method is more practical than considering physical effects, such as the effect of using Maxwell's equations on plasma discharge.

The CEM-P electrode produces corona plasma under atmospheric conditions. Corona plasma is a form of cold plasma that produces reactive oxygen-nitrogen species (RONS) in atmospheric conditions. In industrial interests, RONS can be used to improve post-harvest quality [17], food quality and safety management [18] and so on.

The research results are a graph of the current-voltage characteristics of the corona plasma discharge with a high degree of correspondence between numerical calculations and experimental data (82.35% - 94.44%). The value of the research errors includes standard deviation values between 1.4871-3.3546 and t-test values which are almost all below the value of 0.5 (only one research data with a t-test value=0.5). This (CEM-P) electrode configuration model uses four variations of the sharp angle at the tip of the active electrode ($\phi = 2\theta$) and two variations of the distance between the active and passive electrodes for any given θ value. The value of the resulting corona discharge current is a function of the voltage difference ΔV, the angle and geometric size of the active electrode, and the distance between the active and passive electrodes.

These electrodes model consists of a pair of electrodes positioned perpendicular to each other in the air. These electrodes couple consist of an active electrode shaped like a Pentagonal thin plate, and the mid-sharp end is directed downward in a vertical position. In contrast, a passive electrode is horizontally shaped under the active electrode.

The paper's layout has a structure through the following chapters:

a. Abstract contains a brief explanation of the background, research objectives, research methods, and research results.
b. Introduction contains the background and importance of this research on technological and industrial developments, the background of previous research, research methods, research objectives, research gaps, reasons, and motivations for research.
c. Mathematical model contains a detailed explanation physically and mathematically that relates the concept of electric current formulation from plasma discharge with other variables such as voltage and capacitance value. The capacitance value is determined by the length measurements of the electrode components and the value of k.
d. The technical experiment explains the electronic circuits and equipment used in this research.
e. Results of Simulation and Experiments explain the study of four different sizes of electrode models through the depiction of the (*I-V*) characteristic graphs and their uncertainty errors related to the degree of correspondence between numerical calculations and research data.
f. Discussion contains a discussion of the analysis of the (*I-V*) characteristic graph and the value of the error based on physical and mathematical reasons.
g. Conclusion contains a discussion about the feasibility level of this study based on the research results and discussions that have been presented previously.
h. Acknowledgment and References.

2. MATHEMATICAL MODELS

The (*I-V*) characteristic model in the case of corona plasma discharge expressed in terms of the current function as a function of the square of V has two equations. The first form of this model is as follows:

$$I = CV\left(V - V_i\right) \tag{1}$$

where, I is the corona plasma current, V is the applied voltage, V_i is the initial voltage, and C is the constant. Some of the proponents of the Eq. (1) model include [5, 8, 19-21]. The form of the constant C in Eq. (1) is a function of geometry [8]. The next model of the (*I-V*) characteristic, as proposed [7, 14, 15, 22], has the equation form as:

$$I = C\left(V - V_i\right)^2 \tag{2}$$

This study will use the Eq. (2) model as a reference in the calculation of the (*I-V*) characteristic model, with constant C being a geometric function of the capacitance as proposed by [14, 15]. The capacitance function in the corona discharge is different from the capacitance function in the case of ordinary electricity [23, 24]. The electrode active of the CEM-P configuration has a pentagonal shape. The width and length of the rectangular plate are a and b, respectively, while the width and sharp angle of the triangular plate are d and 2θ, respectively. In comparison, the thickness of the electrode active is skinny ($\delta \cong 0.00015$ meters). The distance between the lower end of electrode active and electrode passive is equal to c. The Electrode passive has a rectangular plane

configuration with a big area to accommodate all the flow of electric plasma flux from the electrode active to the electrode passive. If a dc voltage difference of V between the two electrodes is attached, then a corona plasma discharge event can be created, producing an electric current. The electrode scheme with the CEM-P configuration is found in Figure 1 (a).

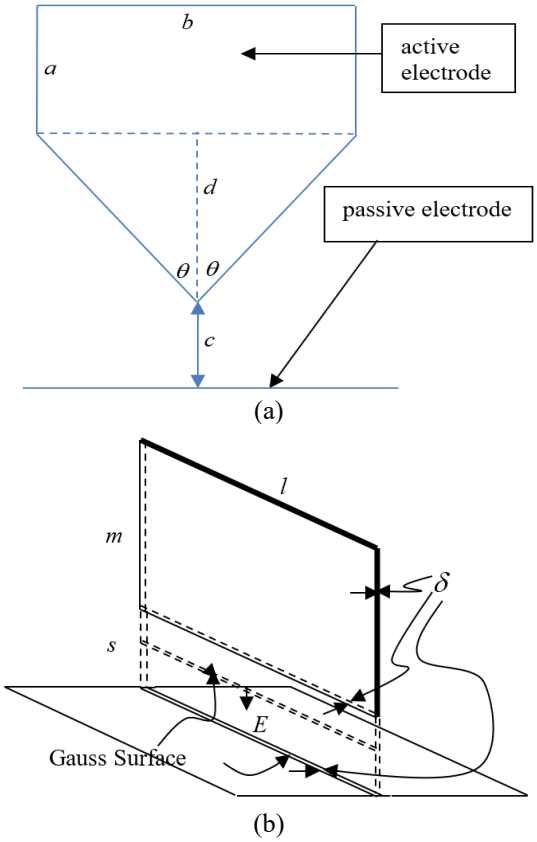

Figure 1. The electrode model Illustration for (a) the CEM-P configuration, (b) the L-P Configuration [14, 15]

Figure 1 (a) is a two-dimensional representation of the CEM-P electrode configuration model. According to geometric calculations, the most significant plasma flow will come out from the lower center end of the pointed active electrode. Furthermore, a smaller stream of plasma will come out of the pointed end of the electrode on both sides of the active electrode. In comparison, the most negligible flow will come out of the sharp lower triangular surface of the active electrode. A passive electrode will accommodate all the plasma flow under the active electrode. For the calculation of the capacitance model of the active electrode system, it has two conditions, namely:

a. For plasma flow straight down, the pentagon-shaped capacitance calculation is transformed into rectangular and triangular capacitances.

b. For the plasma flow coming out of the left and right sides of the active electrode, the capacitance value will be calculated using the integration technique of the capacitance elements.

Before calculating the capacitance value of the electrode model with the CEM-P configuration, a simpler electrode model is needed as the basis for calculating the CEM-P configuration model, namely the electrode model with the Line-Plane (*L-P*) configuration [14, 15]. This electrode model consists of two rectangular plates in a mutually perpendicular position in the air. The active electrode has the area of the rectangle as *lm* (*l* and *m* are the lengths and width values of the plate, respectively) in a vertical position above the passive electrode, which is in a horizontal position. These plates have a thin thickness δ, and the distance between the two plates is *s*, as shown in Figure 1 (b).

The total capacitance value of the electrode model with the *L-P* configuration [14, 15], can be written as:

$$C_{LP} = \varepsilon_0 \, l \ln \left| \frac{m+s}{s} \right| \tag{3}$$

where, ε_0 is the vacuum permittivity. By using formulation (3), we can derive the formulation of the capacitance element from the electrode model with the CEM-P configuration as shown in Figure 2 (a).

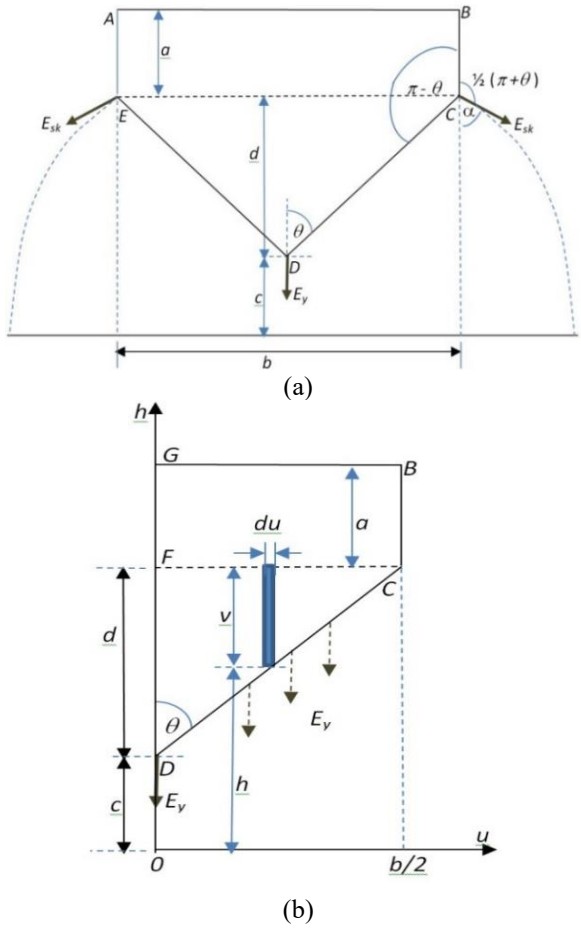

Figure 2. (a) Calculation of the corona plasma discharge electrode's capacitance with the CEM-P configuration has three plasma flows: the lower oblique of the right and left; and straight downward, (b) The plasma flows are calculated straight down, taking only half the right part of the plate. The enormous plasma flow is the one coming out of point *D*

Figure 2 (a) shows the CEM-P electrode configuration model with plate 1 in the shape of an *ABCDE* five-angle plate in an upright position to plate 2, lying horizontally. In this study, the plasma flow was thought to have multiple flow directions that were visible out of some of the sharp surfaces of the electrodes. The flow direction is straight down (seen clearly out of point *D*) and towards the left oblique (seen at point *E*), and oblique to the right (seen at point *C*). Figure 2 (b) shows the calculation model of the plasma flow, which is specifically directed downward by taking half part of the electrode because it has a symmetrical character between the

right and left sides of the *ABCDE* five-angle plate.

The *ABCDE* five-angle plate can be divided into two symmetrical plate areas, where half of the *ABCDE* plate consists of a *GBCF* rectangular plate and an *FDC* triangle. By adopting the Eq. (3) in Figure 2 (b), the capacitance calculation of the *GBCF* rectangular plate electrode will produce a value:

$$C_{1A} = \varepsilon_0 \left(\frac{b}{2}\right) \ln \left| \frac{a+c+d}{c+d} \right| \tag{4}$$

To calculate the electrode capacitance value of the *FDC* triangular plate, we can make a comparison of the *FDC* triangular plate elements with the Eq. (3) so that the value of the capacitance element along with the boundary condition of variable *u* is obtained as:

$$dC_{1B} = \varepsilon_0 \, du \ln \left| \frac{v+h}{h} \right| ; \; 0 \le u \le \tfrac{1}{2} b \tag{5}$$

where, there is a relationship:

$$d+c=v+h \text{ and } \; v = \frac{2ud}{b} \tag{6}$$

The variables *v* and *h* in Eq. (5) can be made as a function of *u* using Eq. (6). The capacitance value calculating results of the FDC triangle plate in Eq. (5) through the concept of integration is:

$$\begin{aligned} C_{1B} = & \left\{ \varepsilon_0 \frac{b}{2d}(c+d) - \varepsilon_0 \frac{bc}{2d} \ln|c+d| \right\} \\ & + \left\{ c\varepsilon_0 \frac{b}{2d} \ln|c| - c\varepsilon_0 \frac{b}{2d} \right\}. \end{aligned} \tag{7}$$

From the comparison of Figures 2 (a) and 2 (b), the *ABCDE* plate's capacitance value is two times that of the *GBCDF* plate. However, if the multiplier factor *k* is entered in the sharp surface around point *D* or at the limit condition *u*=0 in Figure 2 (b), then the capacitance value involving the *ABCDE* plate in the plasma flow downward is:

$$\begin{aligned} C_1 = & \varepsilon_0 \, b \ln \left| \frac{a+c+d}{c+d} \right| + \frac{\varepsilon_0 b}{d} \left[c+d-c\ln|c+d| \right] \\ & + \lim_{k \to \text{big value}} k \frac{\varepsilon_0 bc}{d} \left[\ln|c| - 1 \right]. \end{aligned} \tag{8}$$

In the case of plasma flow out of the left and right oblique directions (points *E* and *C*) from the *ABCDE* plate in Figure 2 (a), then plasma flow depiction for the case half the portion of the total *ABCDE* plate (i.e., *GBCDF* plate) is shown in Figure 3(a). From point *C* in the GBCDF plate, we assumed that there is a plasma flow that is curved at an angle of 60° (considered the mean angle of the observations) so that in the end, the plasma flow reaches the second plate (the passive electrode). The concept of plasma flow from the *GBCDF* plate in Figure 3 (a) will be easier to calculate if a simplification is made with the plate position on the *u-h* coordinate axis, respectively, on the horizontal and vertical coordinate axes as shown in Figure 3 (b). Point *C* on the *GBCDF* plate is the tip of the sharp electrode surface that delivers a more significant amount of plasma than any other surface.

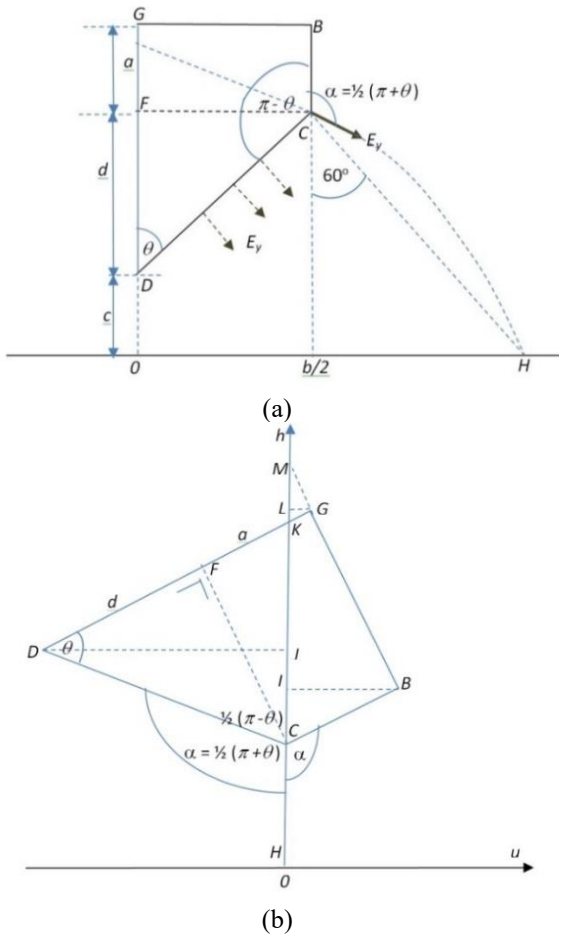

Figure 3. (a) The plasma outflows right obliquely from point *C*. The horizontal length of the plasma path on plate 2 is *l* sin 60°, where *l* is the straight distance from the plasma path that exits from point *C* to the end of the *H* line, and the angle 60° is the mean angle of the observations, (b) The capacitance calculation model with a curved path *CH* is considered a straight line and functions as the vertical coordinate axis of variable *h* with the horizontal coordinate axis of variable *u*

In the case of the CCP electrode, the sharper the electrode shape (the angle is getting taper), the plasma flow is also more excellent (which is indicated by the increasing value of *k*), so there is a relationship as $k \cong 1/\phi$, where ϕ is the acute angle at the end of the CCP electrode emitting plasma flow. If at point *C* which has an acute angle of 2θ and the multiplier factor of shape sharpness is *k*, then the magnitude of the shape sharpness factor at point *C* or *E* is equal to $k_1 = 2\theta k/(\pi - \theta)$.

The total capacitance in the case of plasma flow coming out of the right oblique electrode in Figure 3 (a) (with the depiction of the capacitance triangle in Figure 3 (b) is:

$$\begin{aligned} C_2 = & \left(\frac{2\theta}{\pi-\theta}\right) k \, C_{\text{CBI}} + \left(\frac{2\theta}{\pi-\theta}\right) k \, C_{\text{CDJ}} \\ & + C_{\text{JDK}} + C_{\text{IBM}} - C_{\text{KGL}} - C_{\text{LGM}}. \end{aligned} \tag{9}$$

The multiplier factor k_1 is added to the capacitance-capacitance values of C_{CBI} and C_{CDJ} because the two electrodes are at the sharp end of the electrode at point *C*. The calculation of capacitance from C_{CBI} is based on the concept of the image in Figure 4.

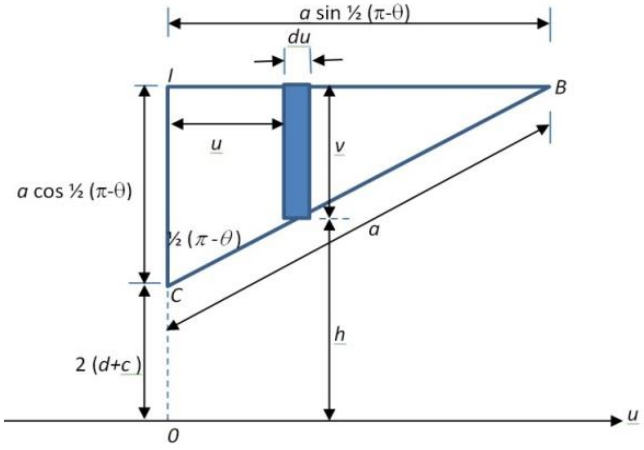

Figure 4. The concept of calculating the capacitance of an electrode C_{CBI}

By comparing the triangles and the same height limit from Figure 4, the values of v and h are obtained as:

$$\begin{aligned} v &= \tan\left(\tfrac{1}{2}\theta\right)\left[d\sec\theta\cos\left(\tfrac{1}{2}\theta\right)-u\right], \\ h &= 2(d+c)+u\tan\left(\tfrac{1}{2}\theta\right). \end{aligned} \tag{10}$$

Through the formulation of the capacitance element and the boundary conditions of the variable u as:

$$dC_{CBI} = \varepsilon_0\, du \ln\left|\frac{v+h}{h}\right|,\ 0\le u\le a\cos\left(\tfrac{1}{2}\theta\right). \tag{11}$$

We get the value of the capacitance C_{CBI} as:

$$\begin{aligned} C_{CBI} &= \varepsilon_0 a\cos\left(\tfrac{1}{2}\theta\right) \\ &\quad -2\varepsilon_0(d+c)\cot\left(\tfrac{1}{2}\theta\right)\ln\left|\frac{2(d+c)+a\sin\left(\tfrac{1}{2}\theta\right)}{2(d+c)}\right|. \end{aligned} \tag{12}$$

The calculation of units along with other capacitance values from Eq. (9) can be seen in Tables 1 and 2. Using Eqns. (9), (12) and Table 2, then the capacitance part value is obtained in the case of plasma flow coming out of the right oblique direction of the electrode, as:

$$\begin{aligned} C_2 = \left(\frac{2\theta}{\pi-\theta}\right)k\Bigg\{ & \varepsilon_0 d\sec\theta\cos\tfrac{1}{2}(\theta)\ln\left|\frac{2(d+c)+d\sec\theta\sin\tfrac{1}{2}(\theta)}{2(d+c)-d\sec\theta\sin\tfrac{1}{2}(\theta)}\right|+\varepsilon_0 a\cos\left(\tfrac{1}{2}\theta\right) \\ & +2\varepsilon_0(d+c)\cot\left(\tfrac{1}{2}\theta\right)\ln\left|\frac{2(d+c)-d\sec\theta\sin\tfrac{1}{2}(\theta)}{2(d+c)+a\sin\left(\tfrac{1}{2}\theta\right)}\right|+\varepsilon_0 d\sec\theta\cos\tfrac{1}{2}(\theta)\Bigg\} \\ & -\varepsilon_0\left[2(d+c)\tan\tfrac{1}{2}(\theta)+a\sin\tfrac{1}{2}(\theta)\tan\tfrac{1}{2}(\theta)+a\cos\tfrac{1}{2}(\theta)\right]\ln\left|2(d+c)+a\sin\tfrac{1}{2}(\theta)\right| \\ & -\varepsilon_0\left[4(d+c)\cot\left(\tfrac{1}{2}\theta\right)+4d\sec\theta\cos\left(\tfrac{1}{2}\theta\right)\right]\ln\left|2d\sec\theta\sin\left(\tfrac{1}{2}\theta\right)+2(d+c)\right| \\ & +\varepsilon_0\left[2(d+c)\cot\left(\tfrac{1}{2}\theta\right)+3d\sec\theta\cos\tfrac{1}{2}(\theta)\right]\ln\left|3d\sec\theta\sin\left(\tfrac{1}{2}\theta\right)+2(d+c)\right| \\ & -\varepsilon_0 d\sec\theta\cos\tfrac{1}{2}(\theta)\ln\left|\,d\sec\theta\sin\tfrac{1}{2}(\theta)+2(d+c)\,\right| \\ & +\varepsilon_0\begin{bmatrix}2(d+c)\tan\left(\tfrac{1}{2}\theta\right)+a\sin\left(\tfrac{1}{2}\theta\right)\tan\left(\tfrac{1}{2}\theta\right)\\ +a\cos\left(\tfrac{1}{2}\theta\right)-2(d+c)-2d\sec\theta\sin\tfrac{1}{2}\theta\end{bmatrix}\ln\left|2(d+c)+(a+d+d\sec\theta)\sin\left(\tfrac{1}{2}\theta\right)\right| \\ & +\varepsilon_0\left[a\sin\tfrac{1}{2}(\theta)-a\cos\left(\tfrac{1}{2}\theta\right)\right]\ln\left|a\cos\tfrac{1}{2}(\theta)\cot\tfrac{1}{2}(\theta)+2(d+c)+a\sin\tfrac{1}{2}(\theta)\right| \\ & +\varepsilon_0\begin{bmatrix}2(d+c)\cot\left(\tfrac{1}{2}\theta\right)+2d\sec\theta\cos\left(\tfrac{1}{2}\theta\right)\\ +2(d+c)+2d\sec\theta\sin\tfrac{1}{2}\theta\end{bmatrix}\ln\left|\begin{matrix}2(d+c)+2d\sec\theta\sin\left(\tfrac{1}{2}\theta\right)+2(d+c)\tan\left(\tfrac{1}{2}\theta\right)\\ +2d\sec\theta\sin\tfrac{1}{2}\theta\tan\left(\tfrac{1}{2}\theta\right)\end{matrix}\right| \\ & -\varepsilon_0(d+d\sec\theta)\tan\left(\tfrac{1}{2}\theta\right)\sin\left(\tfrac{1}{2}\theta\right)-\varepsilon_0 d\sec\theta\cos\left(\tfrac{1}{2}\theta\right)-2\varepsilon_0(d+c)+2\varepsilon_0 d\sec\theta\sin\left(\tfrac{1}{2}\theta\right) \end{aligned} \tag{13}$$

Table 1. Some capacitance boundary conditions for the triangular electrodes indexes name *CDJ*, *JDK*, *IBM*, *KGL* and *LGM*

No.	Indexes name	*v*	*h*	Boundary conditions of *u*
1	*CDJ*	$d\sec\theta\sin\left(\tfrac{1}{2}\theta\right)-\tan\left(\tfrac{1}{2}\theta\right)u$	$2(d+c)+u\tan\left(\tfrac{1}{2}\theta\right)$	$-d\sec\theta\cos\left(\frac{1}{2}\theta\right)\le u\le 0$
2	*JDK*	$d\sec\theta\sin\left(\tfrac{1}{2}\theta\right)-\tan\left(\tfrac{1}{2}\theta\right)u$	$2(d+c)+d\sec\theta\sin\left(\tfrac{1}{2}\theta\right)$	$-d\sec\theta\cos\left(\tfrac{1}{2}\theta\right)\le u\le 0$
3	*IBM*	$a\cot\left(\tfrac{1}{2}\theta\right)\cos\left(\tfrac{1}{2}\theta\right)-u\cot\tfrac{1}{2}(\theta)$	$2(d+c)+a\sin\left(\tfrac{1}{2}\theta\right)$	$0\le u\le a\cos\left(\tfrac{1}{2}\theta\right)$
4	*KGL*	$(a+d-d\sec\theta)\sin\left(\tfrac{1}{2}\theta\right)$ $-u\tan\left(\tfrac{1}{2}\theta\right)$	$2(d+c)+u\tan\left(\tfrac{1}{2}\theta\right)$ $+2d\sec\theta\sin\left(\tfrac{1}{2}\theta\right)$	$0\le u\le 2(d+c)+2d\sec\theta\sin\left(\tfrac{1}{2}\theta\right)$
5	*LGM*	$\left[a\cos\left(\tfrac{1}{2}\theta\right)-u\right]\cot\left(\tfrac{1}{2}\theta\right)$ $-(d+d\sec\theta)\sin\left(\tfrac{1}{2}\theta\right)$	$2(d+c)+$ $(a+d+d\sec\theta)\sin\left(\tfrac{1}{2}\theta\right)$	$2(d+c)+a\sin\left(\tfrac{1}{2}\theta\right)+a\cos\left(\tfrac{1}{2}\theta\right)\cot\left(\tfrac{1}{2}\theta\right)$ $\le u\le 2(d+c)+(a+d+d\sec\theta)\sin\left(\tfrac{1}{2}\theta\right)$

Table 2. Some capacitance values for the triangular electrodes

No.	Indexes name	The triangle capacitance value
1	*CDJ*	$\varepsilon_0 d\sec\theta\cos\frac{1}{2}(\theta)\ln\left\lvert\frac{2(d+c)+d\sec\theta\sin\frac{1}{2}(\theta)}{2(d+c)-d\sec\theta\sin\frac{1}{2}(\theta)}\right\rvert+\frac{2\varepsilon_0(d+c)}{\tan\frac{1}{2}(\theta)}\ln\left\lvert\frac{2(d+c)-d\sec\theta\sin\frac{1}{2}(\theta)}{2(d+c)}\right\rvert$ $+\varepsilon_0 d\sec\theta\cos\frac{1}{2}(\theta)$
2	*JDK*	$2\varepsilon_0 d\sec\theta\cos\frac{1}{2}(\theta)\ln\left\lvert 3d\sec\theta\sin\left(\frac{1}{2}\theta\right)+2(d+c)\right\rvert-\varepsilon_0 d\sec\theta\cos\frac{1}{2}(\theta)\ln\left\lvert 2d\sec\theta\sin\left(\frac{1}{2}\theta\right)+2(d+c)\right\rvert$ $+\left[2\varepsilon_0(d+c)\cot\left(\frac{1}{2}\theta\right)+\varepsilon_0 d\sec\theta\cos\left(\frac{1}{2}\theta\right)\right]\ln\left\lvert\frac{2d\sec\theta\sin\left(\frac{1}{2}\theta\right)+2(d+c)+d\sec\theta\sin\frac{1}{2}(\theta)}{d\sec\theta\sin\left(\frac{1}{2}\theta\right)+2(d+c)+d\sec\theta\sin\frac{1}{2}(\theta)}\right\rvert$ $-\varepsilon_0 d\sec\theta\cos\frac{1}{2}(\theta)\ln\left\lvert d\sec\theta\sin\frac{1}{2}(\theta)+2(d+c)\right\rvert-\varepsilon_0 d\sec\theta\cos\frac{1}{2}(\theta)$
3	*IBM*	$\varepsilon_0\left[a\sin\frac{1}{2}(\theta)+2(d+c)\tan\frac{1}{2}(\theta)+a\sin\frac{1}{2}(\theta)\tan\frac{1}{2}(\theta)\right]\ln\left\lvert a\cos\frac{1}{2}(\theta)\cot\frac{1}{2}(\theta)+2(d+c)+a\sin\frac{1}{2}(\theta)\right\rvert$ $-\varepsilon_0\left[2(d+c)\tan\frac{1}{2}(\theta)+a\sin\frac{1}{2}(\theta)\tan\frac{1}{2}(\theta)\right]\ln\left\lvert 2(d+c)+a\sin\frac{1}{2}(\theta)\right\rvert$ $-\varepsilon_0\, a\cos\frac{1}{2}(\theta)\ln\left\lvert 2(d+c)+a\sin\frac{1}{2}(\theta)\right\rvert-\varepsilon_0 a\cos\frac{1}{2}(\theta)$
4	*KGL*	$\varepsilon_0\left[2(d+c)+2d\sec\theta\sin\frac{1}{2}\theta\right]\ln\left\lvert(a+d)\sin\left(\frac{1}{2}\theta\right)+2(d+c)+d\sec\theta\sin\left(\frac{1}{2}\theta\right)\right\rvert$ $+\left[2\varepsilon_0(d+c)\cot\left(\frac{1}{2}\theta\right)+2\varepsilon_0 d\sec\theta\cos\left(\frac{1}{2}\theta\right)\right]\ln\left\lvert 2(d+c)+2d\sec\theta\sin\left(\frac{1}{2}\theta\right)\right\rvert$ $-\begin{bmatrix}2\varepsilon_0(d+c)\cot\left(\frac{1}{2}\theta\right)+2\varepsilon_0 d\sec\theta\cos\left(\frac{1}{2}\theta\right)\\+2\varepsilon_0(d+c)+2\varepsilon_0 d\sec\theta\sin\frac{1}{2}\theta\end{bmatrix}\ln\left\lvert\begin{matrix}2d\sec\theta\sin\left(\frac{1}{2}\theta\right)+2(d+c)\tan\left(\frac{1}{2}\theta\right)\\+2d\sec\theta\sin\frac{1}{2}\theta\tan\left(\frac{1}{2}\theta\right)+2(d+c)\end{matrix}\right\rvert$ $+2\varepsilon_0(d+c)+2\varepsilon_0 d\sec\theta\sin\frac{1}{2}\theta$
5	*LGM*	$\varepsilon_0\begin{bmatrix}2(d+c)\tan\left(\frac{1}{2}\theta\right)+a\cos\left(\frac{1}{2}\theta\right)\\+a\sin\left(\frac{1}{2}\theta\right)\tan\left(\frac{1}{2}\theta\right)\end{bmatrix}\ln\left\lvert\frac{2(d+c)+a\sin\left(\frac{1}{2}\theta\right)+a\cos\left(\frac{1}{2}\theta\right)\cot\left(\frac{1}{2}\theta\right)}{2(d+c)+(a+d+d\sec\theta)\sin\left(\frac{1}{2}\theta\right)}\right\rvert$ $+\varepsilon_0(d+d\sec\theta)\tan\left(\frac{1}{2}\theta\right)\sin\left(\frac{1}{2}\theta\right)-\varepsilon_0 a\cos\left(\frac{1}{2}\theta\right)$

By using the depiction symmetrical nature of the plasma flow of part half electrodes in the downward direction (Figure 2 (b)) and the right oblique direction (Figure 3 (a)) to the depiction total of the electrodes in Figure 2 (a), then we get the total capacitance value of the electrode model with the CEM-P configuration is:

$$C_{tot} = C_1 + 2C_2 \tag{14}$$

where, C_1 and C_2 are the capacitance values in Eqns. (8) and (13), respectively.

The classical Gauss law concept is used to determine the electric current value of the electrode model with the CEM-P configuration. The amount of electric charge flowing between the two electrodes is equal to $q=C_{\text{tot}}\,\Delta V$. The magnitude of the electric field in the air that is perpendicular downward (along the y axis) between two thin plates (plate thickness $\delta\cong 0.00015$ meters) at the position of the plates that are perpendicular to each other, as shown in Figure 1 (a), can be written as [14, 15]:

$$E_y = \frac{q}{\varepsilon_0(\Delta A)} = \frac{C_{tot}\,\Delta V}{\varepsilon_0\left(b\delta+\delta^2\right)} \tag{15}$$

where, the Gauss area is defined as $\Delta A=(b\delta+\delta^2)$ and the notation δ is defined as the thickness value of the active electrode. The voltage difference $\Delta V=V-V_i$, where V is the applied voltage and V_i is the threshold voltage of the corona.

The total value of the electric current that leaves the electrode system with the CEM-P configuration using the concept of geometric calculations can be defined [14, 15]:

$$I = -\frac{\mu_0}{\Delta V}\left(qE_y^{\,2}\right)_{tot} = -\frac{\mu_0\left\{C_{tot}\right\}^3}{\varepsilon_0^{\,2}\left(b\delta+\delta^2\right)^2}\left(V-V_i\right)^2, \tag{16}$$

where, $\varepsilon_0=8.854\times10^{-12}$ F m^{-1} and $\mu_0=4\pi\times10^{-7}$ Hm^{-1}. Eq. (16) is the formulation of the electric current function I as a function of the voltage V that will characterize the (I-V) theoretical curve at the corona plasma discharge case. This study compared the (I-V) curve and the experimental data points. The sharpness factor of geometric shapes k (contained in the formula of C_{tot}), which is obtained fittingly through a comparison of the theory and experiment results, is the multiplication factor of the current in the corona plasma discharges concept when compared to the ordinary electronic circuit's.

3. EXPERIMENT TECHNIQUE

The electronic circuit arrangement of the corona plasma discharge equipment is shown in Figures 5 (a) and 5 (b) and consists of:

1. The HV high-voltage source in the DC generator equipment (voltage 4 kV and frequency 25 kHz) is connected to the electrodes with the CEM-P configuration.
2. The electric current measuring instrument uses an analog Multimeter with SANWA brand (type YX-360TREB,

voltage 220 V, and frequency 50/60 Hz), arranged in series with the main circuit.

3. The potential difference measuring instrument uses a digital multimeter with SANWA brand CD771.
4. HV probe equipment can convert the potential difference in kV into volts. The electric current that goes to the Voltmeter was passed through the HV probe (Maximum Voltage DC 40 kV DC, model number: AC 28 kV PD-28, serial number: 01605733).

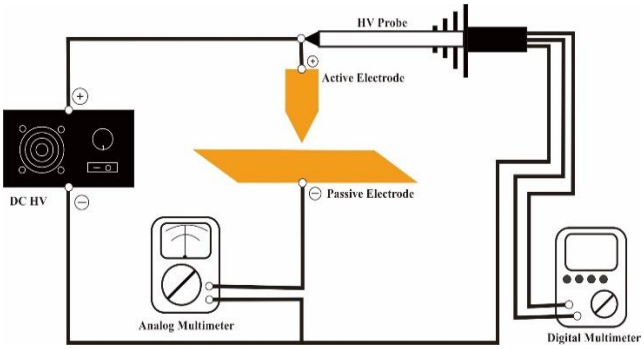

(a)

(b)

Figure 5. (a) and (b) show the circuit schematic and photos of the plasma discharge generator equipment for the CEM-P configuration model, respectively

4. RESULTS OF SIMULATION AND EXPERIMENT

In the plasma discharge experiment of the CEM-P configuration model, the lower triangular ends of the active electrode have four different angle variations. In Figure 2 (a), an active electrode section has several lengths and angles from the pentagon plate. There are several sizes of the same length of the active electrode variations, namely a=0.01 meters, b=0.01 meters and δ=0.00015 meters. While the different sizes (variations) lie in the values of the length d and a half- acute angle θ is:

a. The Electrode Model 1: d=0.010 meters and θ=26,57°
b. The Electrode Model 2: d=0.015 meters and θ=18.44°
c. The Electrode Model 3: d =0.025 meters and θ=11.31°
d. The Electrode Model 4: d=0.030 meters and θ=9.46°

Plasma discharge photos of the four electrode models can be seen in Figure 6.

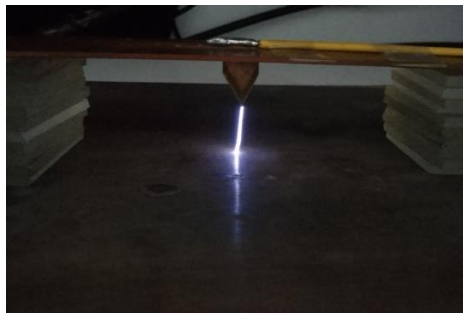

(a) Model 1

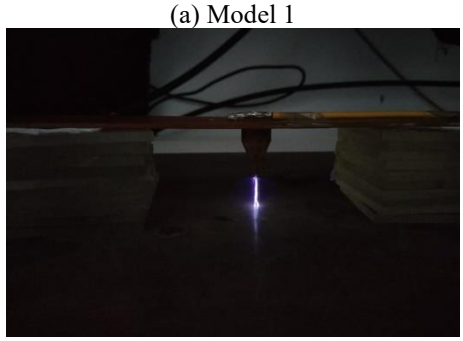

(b) Model 2

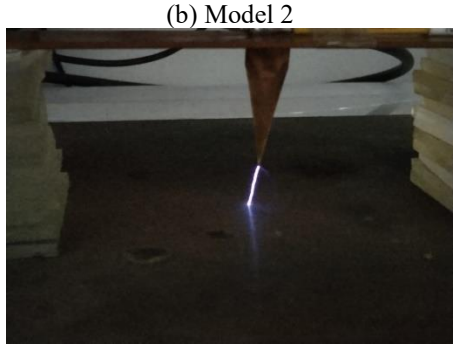

(c) Model 3

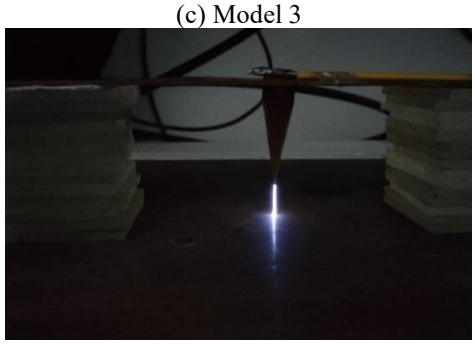

(d) Model 4

Figure 6. The corona discharge photos of four electrode models

The (*I-V*) characteristic graph of the corona discharge case for the CEM-P configuration model was made using the Python Graphical User Interface (*GUI*) Programming [25]. The graph is obtained from the numerical calculations in Eq. (16) for the appropriate value of *k*. Besides describing graphs and calculating the proper *k* value, this GUI program can also calculate graph error values consisting of standard deviation (*SD*) and t-tests. The explanation of the t-test and *SD* values in this study is:

• The t-test value is a parameter that shows the degree of correspondence between the numerical simulation curve and the research data [25] for the (*I-V*) characteristic graph. The smaller the t-test value (which should be less than 0.05), the higher the level of conformity/accuracy between the two functions (simulation curve and research data).

• The value of *SD* (standard deviation) σ_1 in the GUI program for this research comes from the distribution of the measured data up to order of power two of functions *V* in the polynomials [26]:

$$I = a_1 + a_2 V + a_3 V^2 \quad ; \quad \sigma_1 = \sqrt{\frac{\sum_j \left(I - A_1 - A_2 V_j - A_3 V_j^2\right)^2}{(N-2)}}, \tag{17}$$

where, a_1, a_2, and a_3 are constants that can be calculated. The values of A_1, A_2, and A_3 [26] are obtained through Eq. (18):

$$\begin{bmatrix} N & \sum V_j & \sum V_j^2 \\ \sum V_j & \sum V_j^2 & \sum V_j^3 \\ \sum V_j^2 & \sum V_j^3 & \sum V_j^4 \end{bmatrix} \begin{bmatrix} A_1 \\ A_2 \\ A_3 \end{bmatrix} = \begin{bmatrix} \sum I_j \\ \sum V_j I_j \\ \sum V_j^2 I_j \end{bmatrix} \tag{18}$$

The *SD* formula in Eq. (17) is compatible with formula (16) to determine the degree of compatibility between the numerical simulation formula and the research data.

Two (*I-V*) characteristic graphs for each model (with the same angle of θ) are obtained from two variations of *c* values. The *k* factor value, *SD* value, and t-test value are also included in each graph. The display of the (*I-V*) characteristic graphs for the four-electrode models is presented in Figure 7.

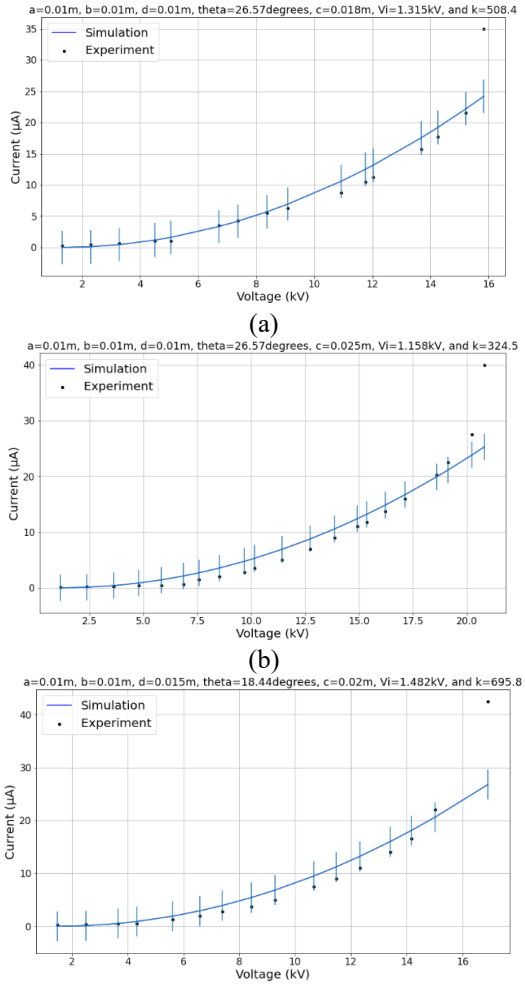

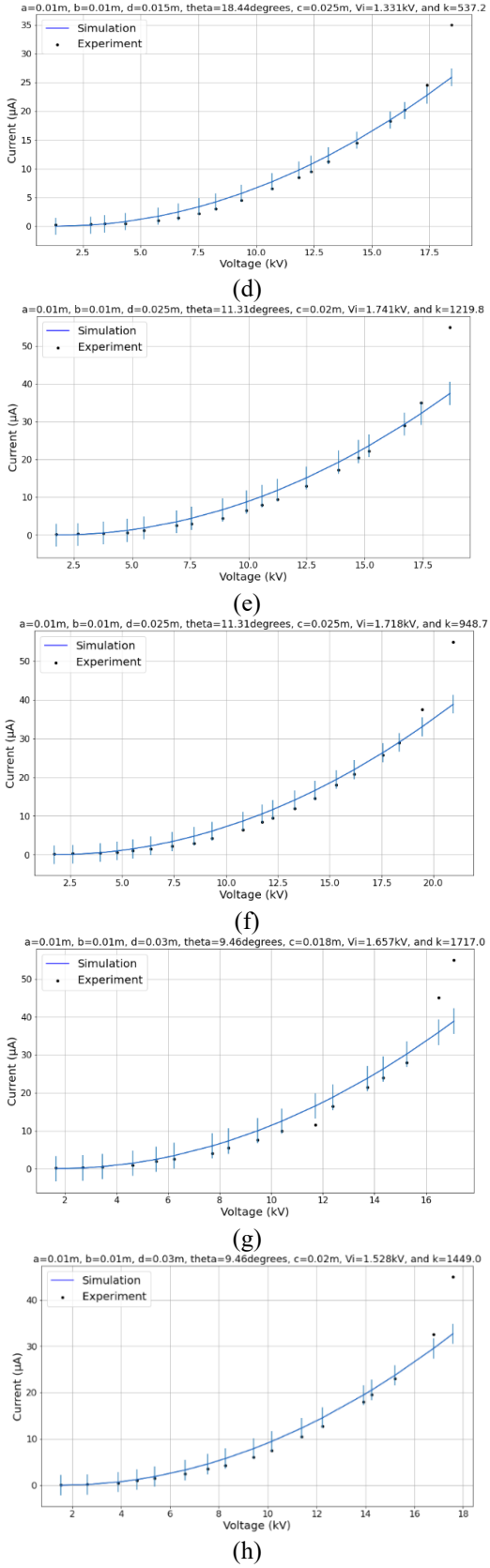

Figure 7. The (*I-V*) Characteristic graph of the corona plasma discharges with the CEM-P configuration at various angles θ and different distances *c*, (a) and (b) are graphs for Model 1 of distances *c*=0.018 m and *c*=0.025 m, respectively (c) and (d) are graphs for Model 2 of distances *c*=0.020 m and *c*=0.025 m, respectively, (e) and (f) are graphs for Model 3 of distances *c*=0.020 m and *c*=0.025 m, respectively, (g) and (h) are graphs for Model 4 of distances *c* = 0.018 m and *c*=0.020 m, respectively

The calculation data for the factor *k*, the *SD* values, and the t-test values in Figure 7 are written in Table 3. On each graph in Figure 7, short vertical lines (*SVL*) connect the data points with the simulation curves. In Figure 7 also, we can manually calculate the values of the number of data points (*NDP*) and the number of tangent points (*NTP*) which is defined as the number of data points that intersect the simulation curve through the *SVL*, and the percentage of tangent points (*PTP*) which is the ratio between *NDP* to *NTP*. A list of the values of *NDP*, *NTP*, and *PTP* is also presented in Table 3.

Table 3. Values of the factor *k*, *SD*, and t-test of the (*I-V*) characteristic functions graphs in Figure 7 for different values of *c*

	Model	*c* (m)	*k*	*SD*	t-test	Number of tangent points	Number of data points	Percentage of tangent points
1	θ=26,57°	0.018	508.4	2.6831	0.0468	15	16	93.75%
		0.025	324.5	2.3665	0.0399	19	21	90.48%
2	θ=18.44°	0.020	695.8	2.8317	0.0496	15	16	93.75%
		0.025	537.2	1.4871	0.0448	17	18	94.44%
3	θ=11.31°	0.020	1219.8	3.0485	0.0475	17	18	94.44%
		0.025	948.7	2.4341	0.0482	18	20	90.00%
4	θ=9.46°	0.018	1717.0	3.3546	0.0481	14	17	82.35%
		0.020	1449.0	2.1841	0.0500	15	17	88.24%

From the (*I-V*) characteristic graph in Figure 7 and from Table 3, which shows the *SD* and the t-test values, as well as from the calculation of the factor *k* based on the variation of the distance between the two electrodes of the *c*, turned out to produce several trends in cases that arise in this study including:

i. The fit between the line simulated curves with the experimental data points occurs in the low-current portion of the corona plasma discharge.
ii. The *SD* values are relatively large for all graphs, whose values vary between 1.4871-3.3546, and the t-test values for almost all graphs are still below 0.5 (except for the case of θ=9.46° with *c*=0.020). Similarly, the whole graph has relatively large *PTP* values (82.35% - 94.44%).
iii. For all variations of the electrodes model, we will see that if the models have a sharper half- acute angle θ, the values of the factor *k* will be greater.
iv. For the case of the same electrodes model, we get research results that the farther the distance between the two electrodes (the greater the value *c*), the values of the factor *k* will be smaller.

5. DISCUSSION

From various research results on the (*I-V*) characteristics of corona discharge such as [5, 6, 19] etc., the level of match between corona current vs voltage occurred only in the case of low current, not in the case of the sharply increasing current. So this study is the same as many cases of previous studies on the (*I-V*) characteristics of corona discharge.

We concluded that the degree of correspondence between the data points and the simulation curve (representing numerical calculation on the Eq. (16)) is relatively high. The statement is based on several measurable categories (use *GUI* programming result) for all graphs in Figure 7, such as:

i. The values of PTP are relatively large (between 82.35% - 94.44%).
ii. The values of the t-test are almost less than 0.5.
iii. Although some factors do not support it, the *SD* values are relatively large (between 1.4871 - 3.3546). The large enough *SD* values mean that the *SVL* sizes are quite long [15].

The best graph in Figure 7 is a combination of low *SD* and t-test values and has a high PTP value, which is suitable for the case of Model 2 (θ=18.44°) at *c*=0.025 m.

The conclusion from the research results [16] is that the sharper the tip of the active electrode used in the case of corona discharge, the larger and brighter the flow of corona current will be. The factor *k* in this study is a multiplier factor of the corona current magnitude that emerges from the lower end of the sharp surface of the active electrode. The concept of the factor *k* is clear based on the research [16]. We conclude that the sharper the tip of the active electrode, the greater the value of the factor *k*.

Another result obtained in this study (in Table 3) is that the greater the value of *c*, the smaller the value of the factor *k*. Figure 6 shows that this study's largest corona current is derived from the corona current coming out of the lower end of the active electrode or out of point *D* in Figure 2 (a). The capacitance value of the area (ΔEDC) = 2×area (Δ *FDC*) in Figure 2, which contains the current multiplier factor *k*, is part of the formulation of Eq. (8) is:

$$C_{EDC} = \lim_{k \to \text{big value}} k \frac{\varepsilon_0 bc}{d}\left[\ln|c| - 1\right]. \quad (19)$$

The values of b and d in Eq. (19) are constant on the change variation of distance c. Suppose it is considered that the C_{EDC} capacitance value is close to a constant on the difference in the value of *c*. In Eq. (19), there is a tendency if the value of c is getting bigger it will make the value of k tend to be smaller, or vice versa if the value of *c* is getting smaller, then the value of *k* tends to be bigger.

6. CONCLUSIONS

The calculation results of the values of the fitting factor *k*, *SD* errors, and t-test in Table 3 for the (*I-V*) characteristics case conclude that there is a high degree of conformity between numerical calculations and research data. This high degree of the agreement indicates that Eq. (16) is suitable as a general formulation of the (*I-V*) characteristics for the corona plasma discharge model with the Chisel Eye and Midpoint-Plane (CEM-P) electrode configuration. However, there may be deviations from the research results stemming from the

negligence of the researchers' observations, the imprecision and asymmetry of the shape and position of the active electrode installation, energy leakage, and other problems that may occur from the physical properties of the corona discharge case.

ACKNOWLEDGMENT

The financials in this work get supported by non-tax revenue (PNBP), Diponegoro University, Semarang, Indonesia, with the schema of International Publication Research (RPI) in 2022. (No. 569-100/UN7.D2/PP/VII/2022).

REFERENCES

[1] Stambouli, A.B., Benallal, R., Oudini, N., Mesli, S.M., Tadjine, R. (2017). Control of dual frequency capacitively coupled plasma via blocking capacitor and phase angle. European Physical Journal Applied Physics, 80: 10802. https://doi.org/10.1051/epjap/2017170180

[2] Tabares, F.L., Junkar, I. (2021). Cold plasma systems and their application in surface treatments for medicine. Molecules, 26(7). https://doi.org/10.3390/molecules26071903

[3] Saikia, P., Bhuyan, H., Escalona, M., Favre, M., Wyndham, E., Maze, J., Schulze, J. (2018). Study of dual radio frequency capacitively coupled plasma: An analytical treatment matched to an experiment. Plasma Sources Science and Technology, 27(1): 015014. https://doi.org/10.1088/1361-6595/aaa565

[4] Townsend, J.S. (1914). The potentials requires to maintain currents between coaxial cylinders. The London, Edinburgh, and Dublin Philosophical Magazine and Journal of Science, 28: 83-90. https://doi.org/10.1080/14786440708635186

[5] Robinson, M. (1967). The corona threshold for coaxial cylinders in air at high pressures. IEEE Transactions on Power Apparatus and Systems, Pas-86: 185-189. https://doi.org/10.1109/TPAS.1967.291834

[6] Zheng, Y., Zhang, B., He, J. (2015). Current-voltage characteristics of dc corona discharges in air between coaxial cylinders. Physics of Plasmas, 22: 023501. https://doi.org/10.1063/1.4907234

[7] Guan, Y., Vaddi, R.S., Aliseda, A., Novosselov, I. (2018). Analytical model of electrohydrodynamic flow in corona discharge. Physics of Plasmas, 25: 083507. https://doi.org/10.1063/1.5029403

[8] Robinson, M. (1961). Movement of air in the electric wind of the corona discharge. Transactions of the American Institute of Electrical Engineers, 80: 143-150. https://doi.org/10.1109/TCE.1961.6373091

[9] Abe, H., Yoneda, M., Fujiwara, N. (2008). Developments of plasma etching technology for fabricating semiconductor devices. Japanese Journal of Applied Physics, 47(3): 1435-1455. https://doi.org/10.1143/JJAP.47.1435

[10] Vidaurre, E.F.C., Achete, C.A., Gallo, F., Garciam D., Simão, R.A., Habert, A.C. (2002). Surface modification of polymeric materials by plasma treatment. Materials Research, 5(1): 37-41. https://doi.org/10.1590/S1516-14392002000100006

[11] Anders, A. (2005). Plasma and ion sources in large area coatings: A review. Surface and Coatings Technology, 200: 1893-1906. https://doi.org/10.1016/j.surfcoat.2005.08.018

[12] Schmidt, H., Sansonnens, L., Howling, A.A., Hollenstein, C., Elyaakoubi, M., Schmitt, J.P.M. (2004). Improving plasma uniformity using lens-shaped electrodes in a large area very high frequency reactor. Journal of Applied Physics, 95: 4559-4564. https://doi.org/10.1063/1.1690096

[13] Bouremel, Y., Li, J.M., Zhao, Z., Debiasi, M. (2013). Effects of AC dielectric barrier discharge plasma actuator location on flow separation and airfoil performance. Procedia Engineering, 67: 270-278. https://doi.org/10.1016/j.proeng.2013.12.026

[14] Wardaya, A.Y., Muhlisin, Z., Hudi, A., Suseno, J.E., Nur, M., Kinandana, A.W., Windarta, J. (2020). A study of line-plane configuration in the Corona discharge theory. The European Physical Journal Applied Physics, 89: 30801. https://doi.org/10.1051/epjap/2020200011

[15] Wardaya, A.Y., Muhlisin, Z., Suseno, J.E., Nur, M., Triadyaksa, P., Khumaeni, A., Sarwoko, E.A., Windarta, J., Hadi, S. (2022). The current-voltage characteristics for electrode geometry model of positive DC corona discharge in air. Gazi University Journal of Science, 35: 1140-1150. https://doi.org/10.35378/gujs.885345

[16] Dobranszky, J., Bernath, A., Marton, H.Z. (2008). Characterisation of the plasma shape of the TIG welding arc. International Journal of Microstructure and Materials Properties, 3(1): 126-140. https://doi.org/10.1504/IJMMP.2008.016949

[17] Hua, X., Li, T., Wu, C., Zhou, D., Fan, G., Li, X., Cong, K., Yan, Z., Wu, Z. (2022). Novel physical treatments (Pulsed light and cold plasma) improve the quality of postharvest apricots after long-distance simulated transportation. Postharvest Biology and Technology, 194(159): 112098. https://doi.org/10.1016/j.postharvbio.2022.112098

[18] Bora, J., Khan, T., Mahnot, N.K. (2022). Cold plasma treatment concerning quality and safety of food: A Review. Current Research in Nutrition and Food Science, 10(2): 427-446. https://doi.org/10.12944/CRNFSJ.10.2.3

[19] Moreau, E., Benard, N., Alicalapa, F., Douyere, A. (2015). Electrohydrodynamic force produced by a corona discharge between a wire active electrode and several cylinder electrodes-Application to electric propulsion. Journal of Electrostatics, 76: 194-200. https://doi.org/10.1016/j.elstat.2015.05.025

[20] Giubbilini, P. (1988). The current-voltage characteristics of point-to-ring corona. Journal of Applied Physics, 64: 3730-3732. https://doi.org/ 10.1063/1.341368

[21] Yamada, K. (2004). An empirical formula for negative corona discharge current in point-grid electrode geometry. Journal of Applied Physics, 96: 2472. https://doi.org/10.1063/1.1775301

[22] Ferreira, G.F.L., Oliveira Jr., O.N., Giacometti, J.A. (1986). Point-to-plane corona: Current-voltage characteristics for positive and negative polarity with evidence of an electronic component. Journal of Applied Physics, 59: 3045-3049. https://doi.org/10.1063/1.336926

[23] Katuri, R., Gorantla, S. (2018). Analysis of math function based controller for a smooth transition between battery and ultracapacitor. Mathematical Modelling of

Engineering Problems, 5(4): 386-394. https://doi.org/10.18280/mmep.050416
[24] Sreedhar, T., Ramana, N.V. (2020). Impact of distribution network reconfiguration and optimal capacitor placement under wheeling transactions. Mathematical Modelling of Engineering Problems, 7(1): 113-118. https://doi.org/10.18280/mmep.070114
[25] Boslaugh, S. (2012). Statistics in a Nutshell: A Desktop Quick Reference. Second Edition. O'Reilly Media, Inc., USA. ISBN-13: 978-1449316822, ISBN-10: 1449316824.
[26] Taylor, J.R. (1997). An Introduction to Error Analysis, the Study of Uncertainties in Physical Measurements. Second Edition. University Science Books, USA. ISBN 0-935702-42-3.

NOMENCLATURE

I	Electric current, Ampere
V	Voltage, Volt
a, b	width and length of the rectangular plate, meters
d	width of the triangular plate, meters
c	distance between the lower end of electrode active and electrode passive, meters
SD	Standard Deviation
k, k_1	shape sharpness factor (dimensionless)
C	constant (the geometric function)
C_1, C_2, ... , C_{tot}	Capacitance, Coulomb/Volt
q	electrical charge, Coulomb
E	electric field, N/C
ΔA	area, m^2

Greek symbols

θ	half- acute angle, radian
δ	plate thickness, meters
σ	standard deviation
ε_0	vacuum permittivity, 8.854×10^{-12} F m^{-1}
μ_0	vacuum permeability, $4\pi\times10^{-7}$ Hm^{-1}
ϕ	acute angle at the end of the CCP electrode emitting plasma flow

Subscripts

i	threshold/initial
j	sum index
tot	total
CBI, CDJ, JDK, IBM, KGL, LGM	triangular electrodes indexes name